Role of the intrinsic charm content of the nucleon from various light-cone models on $\gamma + \mathrm{c}$-jet production

S. Rostami[1)] Muhammad Goharipour[2)] Alireza Aleedaneshvar[3)]

Faculty of Physics, Semnan University, Semnan, P.O. Box 19111-35131, Iran

Abstract: Having a precise knowledge of the charm quark component can lead to a better understanding of the fundamental structure of the nucleon. Furthermore, the charm quark distribution function plays an important role in the study of many processes which are sensitive to the charm quark content of the nucleon. In the standard global analysis of parton distribution functions (PDFs), the charm quark distribution arises perturbatively through the splitting of the gluon into charm-anticharm pairs in the DGLAP evolution equations. Nevertheless, the existence of nonperturbative intrinsic charm quarks in the proton has also been predicted by QCD. In this paper, we study some phenomenological models within the light-cone framework to predict the nonperturbative intrinsic charm quark content of the nucleon. We investigate the impact of these models on the prediction of $\gamma + \mathrm{c}$-jet production in pp collisions at the LHC and compare our results on $\mathrm{p\bar{p}} \to \gamma + \mathrm{c}$-jet with the experimental data of D0.

Keywords: heavy quark PDFs, intrinsic charm, photon production, collider phenomenology

PACS: 12.38.Lg, 12.38.Qk, 13.60.Hb **DOI:** 10.1088/1674-1137/40/12/123104

1 Introduction

A precise knowledge of the parton distribution functions (PDFs) that describe the quark and gluon structure of the nucleon is essential for understanding the interactions of hadrons at high energy, such as those investigated in ep scattering at HERA, $\mathrm{p\bar{p}}$ scattering at the Tevatron, and pp scattering at the LHC. In this vein, the heavy quark components of the nucleon have an important role in testing the perturbative mechanism of Quantum Chromodynamics (QCD) and searching for New Physics. They also play an increasingly significant role for making precise predictions of many new processes, such as single-top and Higgs boson productions in certain scenarios in the standard model (SM) and beyond which are quite sensitive to the charm or bottom quark distributions.

There are several physical observables which are sensitive to the charm quark content of the nucleon and nuclei which can be measured at various colliders such as the Electron-Ion Collider (EIC), Relativistic Heavy Ion Collider (RHIC), Large Hadron electron Collider (LHeC), Tevatron and LHC. Among them, direct photon production in association with a charm quark jet, $\mathrm{h_1 h_2} \to \gamma + \mathrm{c}$-jet, has a very prominent role in providing more information on the charm PDFs. To be more precise, since its cross section is largely dominated by the gluon-charm (gc) channel (as we will explain later), it provides direct access to the gluon and charm distributions in the nucleon and nuclei [1–5]. Experimentally, it has been measured so far only in $\mathrm{p\bar{p}}$ collisions at the Tevatron by the D0 [6, 7] and CDF [8] Collaborations.

In the standard approach for global analysis of PDFs [9–16], the charm quark distribution arises perturbatively through the splitting of the gluons into charm and anticharm pairs in the DGLAP evolution equations [17] and is assumed to be zero for $Q^2 < m_c^2$, where m_c is the charm quark mass. Therefore, we do not need any initial functional form for the charm quark distribution. Nevertheless, there are some experimental data [7, 18] that are sensitive to the charm PDF and suggest the existence of another charm component in the proton called the "intrinsic" charm (IC), since these data cannot be well described by perturbative QCD. In addition to the experimental evidence, the existence of intrinsic charm or generally intrinsic quarks in the proton wave function is predicted theoretically in the light-cone picture of the proton. Note that the intrinsic quarks are certainly nonperturbative in origin and can play an important role at large values of the Bjorken scaling variable x. Nonperturbative intrinsic sea quark components were suggested for the first time by Brodsky, Hoyer, Pe-

Received 24 June 2016, Revised 1 August 2016

1) E-mail: saeedeh.rostami@semnan.ac.ir

2) E-mail: m.goharipour@semnan.ac.ir

3) E-mail: alireza.daneshvar@semnan.ac.ir

terson, and Sakai (BHPS) in 1980 [19]. After considering the intrinsic charm in the proton, they found that its dominant contribution at large x could well explain the unexpected experimental results [20–23] that were larger than the results predicted by conventional QCD calculations.

Over the years, many studies have focused on the intrinsic sea quark components in addition to the commonly perturbative "extrinsic" ones in the nucleon wave function [19, 24–55] (see Refs. [56, 57] for recent reviews). The extrinsic sea quarks arise in the proton perturbatively by gluon splitting and gradually increase when the Q^2 scale increases. The intrinsic sea quarks arise through fluctuations of the nucleon to five-quark states (or virtual meson-baryon states in the meson cloud model (MCM) framework [24–32]) in the light-cone Fock space picture [58]. Meanwhile, the extrinsic sea quarks behave as "sealike" and are the most important at low x. On the contrary, the intrinsic sea quarks have "valence-like" characteristics and then their distributions dominate at relatively large x. In addition to the BHPS model, there have also been some theoretical models based on the light cone framework to describe the IC distribution. Although one can find a review of these models in Refs. [51–53], we will briefly present them in the next section, focusing on their differences.

The probability of investigating intrinsic charm in the nucleon for the first time was given by Brodsky et al. [19] (they estimated it to be around 1%) relying on diffractive production of Λ_c, which is compatible with that of the bag-model [59]. As the first test, Harris et al. [34] performed a global analysis considering the European Muon Collaboration (EMC) data [18], which indicated that an IC component with $0.86\pm0.6\%$ probability can be presented in the nucleon. After that, the CTEQ Collaboration [35, 36] performed a global analysis of PDFs considering the IC component using a wide range of hard-scattering data and found that its probability can even be 2–3 times larger than the BHPS estimation. Recently, two global analyses concerning the probability of IC have been performed. The first one is from the CTEQ Collaboration [37] and follows their previous work (note that in this analysis the EMC data have not been included), and the second is from Jimenez-Delgado et al. [38], using less restrictive cuts to include high-x and low-Q data and also considering the EMC data. In the latter analysis, the probability of IC is reported as 0.5%, which clearly challenges the existence of IC in the nucleon. However, it is indicated that in future, IceCube can constrain the intrinsic charm content of the proton [55].

There are several observables that are sensitive to the charm PDF so that their measurements at large x regions can provide additional unique information about the IC probability. For example, the charm structure function F_2^c from deep inelastic lepton-proton scattering is directly sensitive to the charm distribution through the photon-gluon fusion process $\gamma^*\mathrm{g} \to \mathrm{c\bar{c}}$ at leading-order (LO) and subprocesses $\gamma^*\mathrm{g} \to \mathrm{c\bar{c}g}$ and $\gamma^*\mathrm{q} \to \mathrm{c\bar{c}q}$ at next-to-leading-order (NLO). The only measurement of this quantity at large x was performed by the EMC [18] more than 30 years ago and was recognized as the first evidence for the existence of IC in the proton. The production of charmed hadrons at high x in hadronic or nuclear collisions can also be used in this context, such those measured by the NA3 [60] and R608 [61] Collaborations at CERN and NuSea [62] and E791 [63, 64] Collaborations at FNAL. Furthermore, since the $\gamma+$c-jet production is sensitive to the charm PDF, as mentioned, it can also provide a powerful tool searching for the intrinsic charm components of the nucleon [44, 45] (for the case of intrinsic bottom see Ref. [46]). A similar advantage can be obtained by studying the associated production of a Z boson and a charm quark [47–49, 65].

Although there are some global analyses of PDFs which consider the IC component in the nucleon [35–38], all of them consider only the BHPS model result and the study of other models in a global analysis has not been performed yet. Moreover, there is a limitation in choosing the value of the probability of IC in these analyses. However, it has been indicated that the scale-evolution of the intrinsic heavy quark distributions, to a very good approximation, is governed by non-singlet evolution equations [45, 46]. This allows one to analyse them without having a new global analysis of PDFs. In this paper, we use this technique (the non-singlet evolution) to evolve the intrinsic charm quark distributions from various light-cone models (not only the BHPS) and investigate their impact on the $\gamma+$c-jet production in $\mathrm{p\bar{p}}$ and pp collisions as an example of processes that are sensitive to the charm PDF.

The outline of this paper is as follows. In Section 2, we briefly review the intrinsic charm models based on the light-cone including the BHPS, scalar five-quark and meson-baryon models. The obtained results of these models for IC distribution are also presented at the end of this section. In Section 3, we present our LO and NLO predictions on the production of $\gamma+$c-jet in pp and $\mathrm{p\bar{p}}$ collisions and compare the results of various intrinsic charm models. In particular, we try to investigate which distribution has a better description of D0 data. We summarize our results and present the conclusions in Section 4.

2 The light-cone picture of the proton

In the light-cone framework, the wave function of the proton can be expanded as a sum over the complete or-

thonormal Fock basis of free quarks and gluons such as $|uudg\rangle$, $|uudq\bar{q}\rangle$, etc. [66, 67]. Although, the distribution of q and $\bar{q}$ in the five-quark state $|uudq\bar{q}\rangle$ is predicted in this picture, the magnitude of the probability of this five-quark state cannot be estimated by this picture and is given by another way [35].

Likewise, in the light-cone framework the proton can be pictured as a superposition of configurations of off-shell physical particles such as $p(uud) \to \Lambda_c^+(udc) + \bar{D}^0(u\bar{c})$. One of the unique features of this picture is the difference between c and $\bar{c}$ distributions in the proton. In the following, we review three models of intrinsic charm within the light-cone framework and focus on the differences between the resulting distributions from these models.

2.1 BHPS model

According to the BHPS model, the general form of the distribution for a five-quark Fock state $|uudq\bar{q}\rangle$ by neglecting the effect of transverse momentum is [19]

$$\frac{\mathrm{d}P}{\mathrm{d}x_i\cdots\mathrm{d}x_5}=\mathcal{N}\delta\left(1-\sum_{i=1}^{5}x_i\right)\left[M^2-\sum_{i=1}^{5}\frac{m_i^2}{x_i}\right]^{-2}, \quad (1)$$

where $\mathcal{N}$ is the normalization factor and can be determined from $\mathcal{P}_5^{q\bar{q}}=\int_0^1 \mathrm{d}x_1\cdots\mathrm{d}x_5\mathrm{d}P$. The constant $\mathcal{P}_5^{q\bar{q}}$ is the $|uudq\bar{q}\rangle$ Fock state probability. For the heavy quark c or b denoted by Q, the BHPS model assumes that the light quark and proton masses are negligible compared to the heavy quark mass ($m_Q, m_{\bar{Q}} \gg m_p, m_{q,\bar{q}}$). This assumption simplifies Eq. (1) as follows:

$$\frac{\mathrm{d}P}{\mathrm{d}x_i\cdots\mathrm{d}x_5}=\mathcal{N}_5\delta\left(1-\sum_{i=1}^{5}x_i\right)\frac{x_4^2x_5^2}{(x_4+x_5)^2}, \quad (2)$$

where $\mathcal{N}_5=3600\mathcal{P}_5^{Q\bar{Q}}$. Now, the probability distribution for the intrinsic heavy quark component of the proton is obtained by integrating over $\mathrm{d}x_1\cdots\mathrm{d}x_4$. Considering 1% probability for the IC contribution in the proton, as suggested in Ref. [19], we have

$$\bar{c}(x)=c(x)=18x^2\Big[\frac{(1-x)}{3}(1+10x+x^2) +2x(1+x)\ln(x)\Big]. \quad (3)$$

Although 1% normalization of the IC component was initially anticipated, different values of $\mathcal{P}_5^{c\bar{c}}$ were indicated in several studies [34–38]. It is worth noting here that according to the BHPS model, we have equal probability distributions for c and $\bar{c}$ in the five-quark state $|uudc\bar{c}\rangle$, since we use the same value for the mass of c and $\bar{c}$.

2.2 Scalar five-quark model

A more detailed model to describe the proton in the light-cone was presented by Pumplin [51] in which some simplifying assumptions considered in the BHPS model were removed. In this model, which is called the scalar five-quark model, the probability distribution for the five-quark state derives directly from the Feynman diagram rules. In a simple case, if a point scalar particle of mass M couples to N scalar particles with masses $m_1,\cdots,m_N$ by a point coupling ig, the probability density for the N-quark Fock state can be written as

$$\mathrm{d}P=\mathcal{N}\prod_{i=1}^{N}\frac{\mathrm{d}x_i}{x_i}\delta\left(1-\sum_{i=1}^{N}x_i\right)\prod_{i=1}^{N}\mathrm{d}^2k_{i\perp}\delta^{(2)}\left(\sum_{i=1}^{N}k_{i\perp}\right) \times\frac{F^2(s)}{(s-M^2)^2}, \quad (4)$$

where

$$s=\sum_{i=1}^{N}(m_i^2+k_{i\perp}^2)/x_i, \quad (5)$$

and $\mathcal{N}$ is again the normalization factor. The wave function factor $F^2(s)$ that characterizes the dynamics of the bound state is applied to suppress the contributions from the high-mass configurations. Note that by considering $N=5$ and a point form factor as $F(s)=1$, and also neglecting the $1/x_i$ factors and $k_{\perp i}$ content in Eq. (4), we reach the BHPS probability distribution in Eq. (1). As mentioned above, Pumplin considered further suppression for contributions from high-mass states in addition to the $(s-M^2)^{-2}$ factor to make the integrand probability finite by entering a wave function factor $F^2(s)$. He proposed two exponential and power-law forms for it as follows

$$F^2(s)=\exp[-(s-M^2)/\Lambda^2], \quad (6)$$

$$F^2(s)=(s+\Lambda^2)^{-n}, \quad (7)$$

where Λ is a cutoff mass regulator with range of $\Lambda = 2-10$ GeV [51].

In order to investigate the effects of different shapes for the intrinsic charm distribution on the γ+c-jet cross section, we chose the charm quark momentum distribution of the power-law form with $n=4$ and cut-off parameter $\Lambda=10$ GeV which is shifted to lower x, than the BHPS and $\Lambda=2$ GeV for the exponential form of scalar five-quark model, which is shifted to larger x than the BHPS, as shown in Fig 1. The parametrization forms of the charm distributions in the proton for the exponential and power-law form factors described above are [51]

$$\bar{c}(x)=c(x)=520.517\,x^{4.611}(1-x)^{11.477}, \quad (8)$$

$$\bar{c}(x)=c(x)=0.187\,x^{0.521}(1-x)^{4.194}, \quad (9)$$

where the normalization coefficients are chosen to make the momentum fraction $\int_0^1 f_{c,\bar{c}}(x)x\mathrm{d}x$ equal to 0.002857, a value given by the BHPS model.

2.3 Meson-baryon model

In addition to the BHPS and scalar five-quark models, there is another model in which the nucleon fluctuates to a virtual meson plus a baryon state and is often called the meson cloud model (MCM) or meson-baryon model (MBM) [24–30]. In this case, the wave function of the nucleon is described with

$$|p\rangle = \sqrt{Z}|p\rangle_{\rm bare} + \sum_{M,B}\int {\rm d}y\ {\rm d}^2\boldsymbol{k}_\perp \phi_{MB}(y,k_\perp^2) \times |M(y,\boldsymbol{k}_\perp);B(1-y,-\boldsymbol{k}_\perp)\rangle, \quad (10)$$

where Z is the wave function renormalization constant. $\phi_{MB}(y,k_\perp^2)$ is the wave function of the Fock state containing a virtual meson M with longitudinal momentum fraction y and transverse momentum $\boldsymbol{k}_\perp$ and a baryon B with longitudinal momentum fraction $1-y$ and transverse momentum $-\boldsymbol{k}_\perp$. For example, the contribution to the charm sea in this view can come from a fluctuation such as $p(uud)\to\Lambda_c^+(udc)+\bar{D}^0(u\bar{c})$, so that the contribution to the charm and anticharm quark distributions comes from the charm quark in the Λ_c^+ and anticharm quark in the $\bar{D}^0$, respectively. Finally, the intrinsic charm and anticharm distributions in the proton can be expressed as a convolution of fluctuation functions with the relative valence distributions in the baryon and meson [27]. There is a major difference between the MBM and other models. As mentioned above, since the charm and anticharm have different distributions in the baryon and meson states and the probability distributions of meson and baryon in the proton are also different, the MBM predicts the asymmetry of $c(x)$ and $\bar{c}(x)$ distributions in the proton. Here, we investigate the effects of intrinsic charm quark from two MBM models including the confining model and effective mass model on the cross section of the inclusive production of photon accompanied by a c-jet. The parametrization forms for the intrinsic charm distributions in the nucleon for these models are given, respectively, by [52]

$$c(x) = 4.128\,x^{1.59}(1-x)^{6.586}, \quad (11a)$$

$$\bar{c}(x) = 1.77696\,x^{1.479}(1-x)^{4.624}, \quad (11b)$$

and

$$c(x) = 252.48\,x^{3.673}(1-x)^{10.16}, \quad (12a)$$

$$\bar{c}(x) = 99.84\,x^{4.153}(1-x)^{6.800}. \quad (12b)$$

Figure 1 shows a comparison of intrinsic charm distributions from the BHPS, scalar five-quark and meson-baryon models. The black solid curve represents the result of BHPS (Eq. (1)). The Pumplin models are represented by the blue dash-dotted and green dash-dotted-dotted curves. Note that the exponential form (Eq. (8)) is clearly dominant at larger x while the power-law form (Eq. (9)) is dominant at lower x. Thus it seems that the power-law form can be more important for the Tevatron and LHC predictions. In the case of MBM, the results of c and $\bar{c}$ distributions from the effective mass model (Eq. (12)) represented by the red solid and dashed curves are slightly harder, especially for the $\bar{c}$, compared to the similar cases from the confining model (Eq. (11)) represented by the pink solid and dashed curves. However, both are larger in magnitude than the BHPS and Pumplin models. Therefore, depending on the applied cuts for the transverse momentum and pseudorapidity of photon in $\gamma+$c-jet production, each of them can be important.

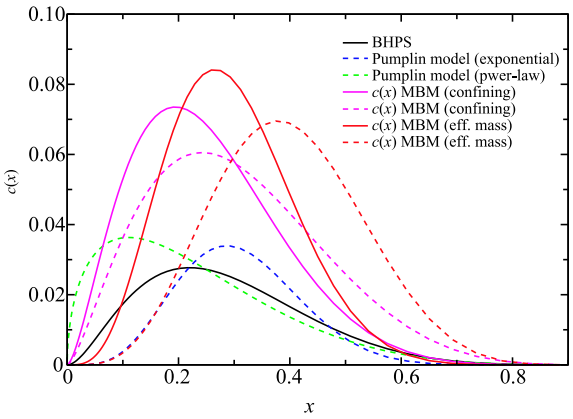

Fig. 1. The momentum distribution of intrinsic c and $\bar{c}$ from the various light-cone models. The black solid curve is the BHPS model result (Eq. (1)). The blue and green dashed-dotted curves are from the exponential (Eq. (8)) and power-law (Eq. (9)) forms of Pumplin model, respectively. The red solid and dashed curves are the results of the confining model of MBM for c and $\bar{c}$ (Eqs. (11a) and (11b)), respectively. Finally, the pink solid and dashed curves are the results of the effective mass model of MBM for c and $\bar{c}$ (Eqs. (12a) and (12b)), respectively.

3 Prompt photon production in association with a c-jet

In this paper, we turn our attention to the prompt photon production in association with a charm quark jet process and investigate the impact of the intrinsic charm quark component in the proton on this quantity for the Tevatron at 1.96 TeV and LHC at 8 and 13 TeV. At LO, the main contribution to the $\gamma+$c-jet production arises from the Compton subprocess $gc\to\gamma c$ (Fig. 2) which dominates at low $p_{\rm T}^\gamma$ [44]. In addition to the Compton subprocess, we have the partonic subprocess light

quark-antiquark annihilation $q\bar{q}\to\gamma g\to\gamma c\bar{c}$. In pp collisions, the Compton process dominates in all energies but the $q\bar{q}$-annihilation subprocess does not play a significant role. In $p\bar{p}$ collisions, the $q\bar{q}$-annihilation subprocess dominates at high photon transverse momentum p_T^γ [2].

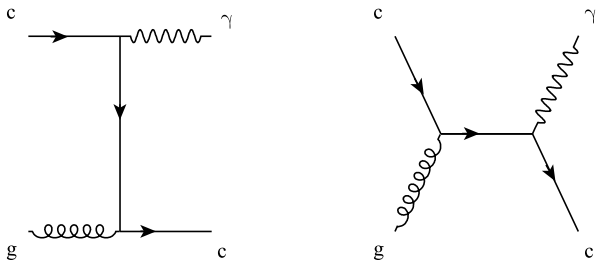

Fig. 2. The t-channel (left) and s-channel (right) Feynman diagrams for the Compton sub-process $gc\to\gamma c$.

At NLO, the process $pp(\bar{p})\to\gamma$+c includes the contributions from the gluon fusion subprocess $gg\to\gamma c\bar{c}$ and $gc\to\gamma qc$ [2, 3]. Since most subprocesses at NLO are g and c initiated, almost all dependencies of the NLO $\gamma+$c-jet cross section to the PDFs come from the gluon and charm PDFs [3].

3.1 Comparison to Tevatron data

The cross section of photon production in association with a heavy quark jet in $p\bar{p}$ collisions has been measured at the Tevatron in recent years [6–8, 68, 69]. In particular, in Ref. [7] the associated production of photons and c-quark jets in $p\bar{p}$ collisions at the center-of-mass energy $\sqrt{s}=1.96$ TeV with photon rapidity $|y^\gamma|<1.0$ and transverse momentum $30<p_T^\gamma<300$ GeV has been measured as a function of p_T^γ so that the c-jets have pseudorapidity $|\eta^c|<1.5$ and transverse momentum $p_T^c>15$ GeV.

Figure 3 shows a comparison of the D0 measurement of the differential $\gamma+$c-jet cross section as a function of p_T^γ [7] and the LO and NLO theoretical predictions. The comparison between the LO calculations using different intrinsic charm models is displayed in the upper panel. All of the above calculations have been carried out by MadGraph [70]. The lowest curve is related to CTEQ66 PDFs [36] without the IC contribution. It is clear that the data are poorly described. At large p_T^γ regions, as expected, the spectrum grows by the inclusion of the IC contribution. It should be noted that the IC contribution from the BHPS model is considered as 1% probability for the intrinsic charm. For the BHPS, the result is improved by a factor of 1.45 at $p_T^\gamma\simeq 216$ GeV compared to the result of pure extrinsic calculation (CTEQ66). These factors for the Pumplin model with the exponential and power-law suppression are about 1.5 and 1.3, respectively. Therefore, the results of the cross section calculation for the BHPS and Pumplin models are almost identical under the limits mentioned.

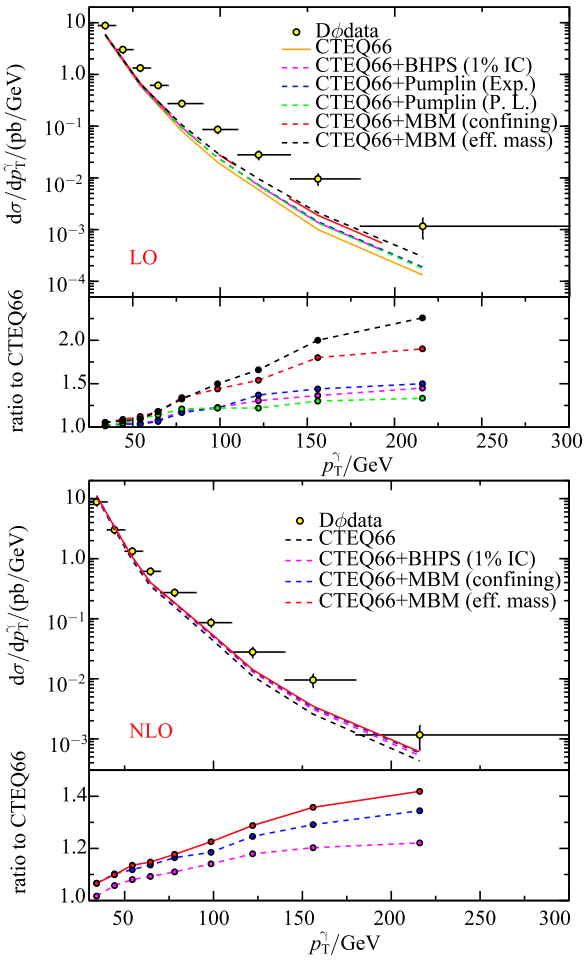

Fig. 3. A comparison of D0 measurement of differential $\gamma+$c-jet cross section as a function of p_T^γ at $\sqrt{s}=1.96$ TeV [7] and corresponding LO (top) and NLO (bottom) theoretical calculations. For both cases, the ratios of the results to the CTEQ66 [36] prediction are shown in the bottom panels. For LO, the solid curve indicates the CTEQ66 (pure extrinsic) result. The dashed, dashed-dotted, dashed-dotted-dotted, dashed-dashed-dotted and dotted curves correspond to the inclusion of IC contribution from the BHPS (with 1% IC), the exponential and power-law forms of Pumplin and the confining and effective mass models of MBM, respectively. For NLO, the dotted curve indicates the CTEQ66 result and the dashed-dotted, dashed and solid curves correspond to the results of the BHPS (with 1% IC), confining and effective mass models, respectively.

One can see from Fig. 3 that the MBM results are much higher than the BHPS and Pumplin results. The MBM contribution increases the spectrum by a factor of 1.9 for the confining model and 2.25 for the effective

mass model at $p_{\rm T}^{\gamma} \simeq 216$ GeV. Nevertheless, the results at LO are below the range of data points and none of the models provide an appropriate description of data.

The NLO results for the calculation of the differential $\gamma+$c-jet cross section in $p\bar{p}$ collisions as a function of $p_{\rm T}^{\gamma}$ are compared to D0 data in the lower panel of Fig. 3. As expected, these results have improved compared to the LO results (upper panel). The same as LO, a growth in spectrum is observed in the NLO by inclusion of the IC contribution at large $p_{\rm T}^{\gamma}$. Note that since the BHPS and Pumplin -whether with the exponential or power-law suppression factor- models provide almost the same result for the cross section under the limits mentioned, only the BHPS and MBM models were considered for the NLO calculations. In this figure, the dotted and dashed-dotted curves represent the theoretical results for the cross section using the CTEQ66 [36] PDFs (without IC contribution) and CTEQ66 plus the BHPS with 1% IC, respectively. The dashed and solid curves indicate the results for the cross section by adding the intrinsic charm distribution from the confining and effective mass models of MBM to the pure extrinsic PDFs of CTEQ66. It should also be noted that there is a significant difference between the BHPS (1% IC) and MBM results, especially at high p_T^{γ}.

3.2 Predictions for the LHC

The LHC with pp collisions operates at the center-of-mass energy $\sqrt{s} = 7-14$ TeV, which is much greater than the Tevatron. In order to study the effects of intrinsic charm quark distribution from various light-cone models on the prediction of the inclusive production of $\gamma+$c-jet at the LHC, we need to select the most sensitive kinematical regions to the IC contribution. For this aim, we use the kinematical regions which were analysed in detail by V. A. Bednyakov et al. [44]. The differential $\gamma+$c-jet cross section in pp collisions versus the transverse momentum of the photon is presented for the photon rapidity $1.52 < |y^{\gamma}| < 2.37$ and transverse momentum $50 < p_{\rm T}^{\gamma} < 400$ GeV at $\sqrt{s} = 8$ TeV. The c-jet also has $|\eta^{\rm c}| < 2.4$ and $p_{\rm T}^{\rm c} > 20$ GeV. In this kinematical region, the charm momentum fraction is larger than 0.1 ($x_{\rm c} > 0.1$) and the intrinsic charm distribution is considerable in comparison with the extrinsic charm distribution. The prediction for the LHC at LO is shown in the upper panel of Fig. 4. In this figure, the difference between the pure extrinsic CTEQ66 result and the results obtained by considering the IC contribution from various models is clearly visible, especially at large $p_{\rm T}^{\gamma}$. Like the results of the Tevatron, at the LHC, the BHPS and Pumplin models give almost the same results. The MBM results at high $p_{\rm T}^{\gamma}$ are higher than the other models, just like the Tevatron case. The ratios of the differential γ+c-jet cross section considering the IC contribution from various models to the CTEQ66 prediction are presented in the bottom of this panel. The inclusion of the confining model of MBM increases the spectrum by a factor of 2.5 at $p_{\rm T}^{\gamma} = 380$ GeV, while for the effective mass model, this factor is about 3.1. Also, considering the IC contribution from Pumplin models with exponential and power-law form factors increase the spectra by a factor of 2.12 and 1.8, respectively.

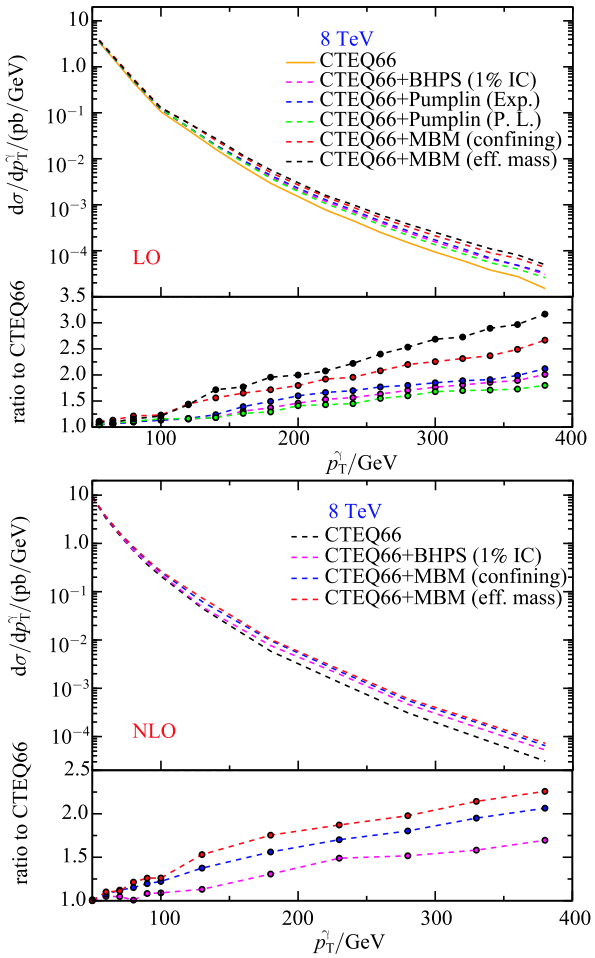

Fig. 4. The LO (top) and NLO (bottom) theoretical predictions for the differential $\gamma+$c-jet cross section in pp collisions as a function of $p_{\rm T}^{\gamma}$ for photon rapidity $1.52 < |y^{\gamma}| < 2.37$ and transverse momentum $50 < p_{\rm T}^{\gamma} < 400$ GeV, and c-jets pseudorapidity $|\eta^{\rm c}| < 2.4$ and transverse momentum $p_{\rm T}^{\rm c} > 20$ GeV at $\sqrt{s} = 8$ TeV. The description of the results is same as Fig. 3.

In the lower panel of Fig. 4, the differential cross section $\mathrm{d}\sigma/\mathrm{d}p_T^{\gamma}$ for pp $\to \gamma+$c-jet process calculated at the NLO is presented as a function of the photon transverse momentum. The NLO results are larger than LO by a factor of 2.07 at $p_{\rm T}^{\gamma} = 380$. Like the Tevatron results, considering the IC contribution can substantially increase the cross section values, especially at high $p_{\rm T}^{\gamma}$. The difference between models is clearly visible in the bottom

of each panel, where the ratios of the spectra including the IC contribution from the various above-mentioned models to the CTEQ66 result are shown as a function of $p_{\rm T}^{\gamma}$. By comparing the results, one can see that the values of the spectra increase when the IC contribution is considered so, that the MBM results are higher than the BHPS with 1% IC result. For example, the inclusion of the BHPS with 1% IC increases the spectrum by a factor of 1.69 at $p_{\rm T}^{\gamma}=380$, while for the effective mass model of MBM this factor is about 2.25.

We now turn our attention to investigate the impact of intrinsic charm component of the proton on the pp $\rightarrow\gamma+$c cross section at the center-of-mass energy $\sqrt{s}=13$ TeV. As described above for the case of $\sqrt{s}=8$ TeV we used the kinematical regions introduced by V. A. Bednyakov et al. [44] for which we have $x_{\rm c}>0.1$ where x_c is the charm momentum fraction in the proton. We can use the following relation to find the favoured kinematical regions for the case of $\sqrt{s}=13$ TeV

$$x_{\rm c}\geqslant x_{\rm F}=\frac{2p_{\rm T}}{\sqrt{s}}\sinh(\eta), \tag{13}$$

where $x_{\rm F}$ is the Feynman scaling of the produced hadron. Actually, the effect of the intrinsic charm in the process pp $\rightarrow\gamma+$c at 13 TeV is similar to that at energy about 8 TeV but at larger values of the photon transverse momentum. To be more precise, if we want to have $x_{\rm c}\geqslant 0.1$, using Eq. 13 the values of the photon transverse momentum $p_{\rm T}$ for $\sqrt{s}=13$ TeV will change by a factor 13/8 in proportion to $\sqrt{s}=8$ TeV.

In Figure 5, we show the theoretical predictions of the differential cross section $\mathrm{d}\sigma/\mathrm{d}p_{\rm T}^{\gamma}$ for the γ+c-jet production in pp collisions at $\sqrt{s}=13$ TeV. The calculations are carried out at NLO in QCD for the photon transverse momentum $80<p_{\rm T}^{\gamma}<540$ GeV. Since the BHPS and Pumplin models have similar results, here we have calculated the cross section only by including the BHPS model and MBM. Like before, we see that the IC contribution can substantially increase the cross section especially at high $p_{\rm T}^{\gamma}$. Moreover, the MBM prediction (whether for the confining or effective mass model) is again higher than the prediction of the BHPS model with 1% probability. The difference between the results is clearly visible at the bottom of Fig. 5 where, the ratios of the spectra including the IC contribution to the CTEQ66 prediction are shown as a function of $p_{\rm T}^{\gamma}$. For example, the inclusion of the IC contribution from the effective mass model of MBM increases the spectrum by a factor 2.4 at $p_{\rm T}^{\gamma}=540$ GeV, while for the BHPS model this factor is about 1.46. This figure clearly shows that the existence of the IC component can be investigated experimentally by measuring the $\gamma+$c-jet production in pp collisions even at very high energies, focusing on the large $p_{\rm T}^{\gamma}$ regions.

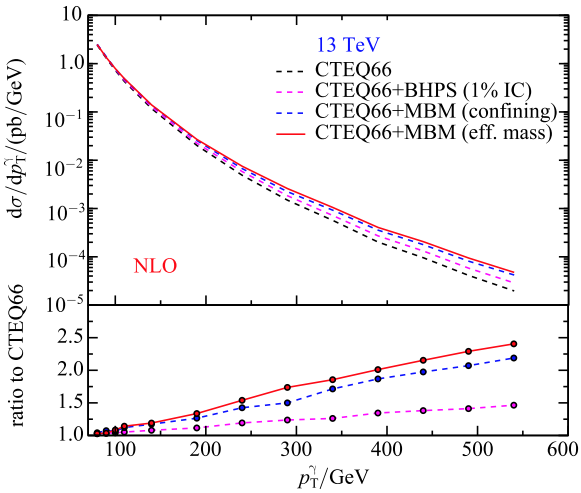

Fig. 5. The NLO theoretical predictions for the differential $\gamma+$c-jet cross section in pp collisions as a function of $p_{\rm T}^{\gamma}$ for the photon rapidity $1.52<|y^{\gamma}|<2.37$ and transverse momentum $80<p_{\rm T}^{\gamma}<540$ GeV at $\sqrt{s}=13$ TeV. The dotted curve indicates the CTEQ66 (pure extrinsic) result. The dashed-dotted, dashed and solid curves correspond to the inclusion of the IC contribution from the BHPS model (with 1% IC), the confining and effective mass models of MBM, respectively. The ratios of the results to the CTEQ66 [36] prediction are shown in the bottom panels.

4 Conclusions

Heavy quark distributions play an important role in the study of many processes and can help to improve our understanding of the fundamental structure of the nucleon. The possible existence of intrinsic heavy quarks in the nucleon, particularly the charm quark, was first suggested by Brodsky et al. [19]. After that, other theoretical calculations such as the scalar five-quark model and meson-baryon model (MBM) have tried to describe the intrinsic charm quark distribution. These models predict different intrinsic charm distributions in the nucleon and may lead to different results for any physical quantity that is sensitive to the charm content of the nucleon. In this work, we performed a comparative analysis of three intrinsic charm models to study the role of intrinsic charm in the results of the inclusive production of a prompt photon in association with a c-jet in hadron colliders. We presented the calculations for the Tevatron $\mathrm{p\bar{p}}$-collisions for rapidity $|y^{\gamma}|<1$, $|\eta^{\rm c}|<1.5$ at $\sqrt{s}=1.96$ TeV and the LHC pp-collisions for $|\eta^{\rm c}|<2.4$ and $1.52<|y^{\gamma}|<2.37$ at $\sqrt{s}=8$ TeV and $\sqrt{s}=13$ TeV. The results were presented at both LO and NLO. We found that, regardless of the chosen intrinsic model, the IC contribution increases the magnitude of the cross section and has a more significant effect at large transverse

momentum of the photon. In these kinematic regions, the BHPS and Pumplin models have the same results. Furthermore, the difference between these two models (with inclusion of 1% IC) and the MBM is clearly visible so that the latter gives a much better description of the D0 data. In general, the MBM prediction is always higher than the predictions of the other models. However, in this work, we considered 1% probability for the IC contribution in the BHPS and Pumplin models, so any variation in the magnitude of this probability absolutely changes these results. We concluded that the existence of IC component can be investigated experimentally by measuring the γ+c-jet production in pp collisions even at very high energies, focusing on the large p_T^γ regions.

References

1 B. Bailey, E. L. Berger, and L. E. Gordon, Phys. Rev. D, **54**: 1896 (1996) [arXiv:9602373 [hep-ph]]
2 T. P. Stavreva and J. F. Owens, Phys. Rev. D, **79**: 054017 (2009) [arXiv:0901.3791 [hep-ph]]
3 T. Stavreva, I. Schienbein, F. Arleo, K. Kovarik, F. Olness, J. Y. Yu, and J. F. Owens, JHEP, **1101**: 152 (2011) [arXiv:1012.1178 [hep-ph]]
4 H. B. Hartanto, FERMILAB-THESIS-2013-37
5 T. Stavreva, F. Arleo, and I. Schienbein, JHEP, **1302**: 072 (2013) [arXiv:1211.6744 [hep-ph]]
6 V. M. Abazov et al (D0 Collaboration), Phys. Rev. Lett., **102**: 192002 (2009) [arXiv:0901.0739 [hep-ex]]
7 V. M. Abazov et al (D0 Collaboration), Phys. Lett. B, **719**: 354 (2013) [arXiv:1210.5033 [hep-ex]]
8 T. Aaltonen et al (CDF Collaboration), Phys. Rev. Lett., **111**: 042003 (2013) [arXiv:1303.6136 [hep-ex]]
9 L. A. Harland-Lang, A. D. Martin, P. Motylinski, and R. S. Thorne, Eur. Phys. J. C, **75**: 204 (2015) [arXiv:1412.3989 [hep-ph]]
10 S. Dulat et al, Phys. Rev. D, **93**: 033006 (2016) [arXiv:1506.07443 [hep-ph]]
11 R. D. Ball et al (NNPDF Collaboration), JHEP, **1504**: 040 (2015) [arXiv:1410.8849 [hep-ph]]
12 S. Alekhin, J. Bluemlein, and S. Moch, Phys. Rev. D, **89**: 054028 (2014) [arXiv:1310.3059 [hep-ph]]
13 P. Jimenez-Delgado and E. Reya, Phys. Rev. D, **89**: 074049 (2014) [arXiv:1403.1852 [hep-ph]]
14 H. Abramowicz et al (H1 and ZEUS Collaborations), Eur. Phys. J. C, **75**: 580 (2015) [arXiv:1506.06042 [hep-ex]]
15 A. Accardi, L. T. Brady, W. Melnitchouk, J. F. Owens, and N. Sato, Phys. Rev. D, **93**: 114017 (2016) [arXiv:1602.03154 [hep-ph]]
16 H. Khanpour, A. N. Khorramian, and S. A. Tehrani, J. Phys. G, **40**: 045002 (2013) [arXiv:1205.5194 [hep-ph]]
17 V. N. Gribov and L. N. Lipatov, Sov. J. Nucl. Phys., **15**: 438 (1972); G. Altarelli and G. Parisi, Nucl. Phys. B, **126**: 298 (1997); Yu. L. Dokshitzer, Sov. Phys. JETP, **46**: 641 (1977)
18 J. J. Aubert et al (European Muon Collaboration), Nucl. Phys. B, **213**: 31 (1983)
19 S. J. Brodsky, P. Hoyer, C. Peterson, and N. Sakai, Phys. Lett. B, **93**: 451 (1980); S.J. Brodsky, C. Peterson, and N. Sakai, Phys. Rev. D, **23**: 2745 (1981)
20 D. Drijard et al (CERN-College de France-Heidelberg-Karlsruhe Collaboration), Phys. Lett. B, **81**: 250 (1979)
21 K. L. Giboni et al, Phys. Lett. B, **85**: 437 (1979)
22 W. S. Lockman, T. Meyer, J. Rander, P. Schlein, R. Webb, S. Erhan, and J. Zsembery, Phys. Lett. B, **85**: 443 (1979)
23 D. Drijard et al (ACCDHW Collaboration), Phys. Lett. B, **85**: 452 (1979)
24 A. W. Thomas, Phys. Lett. B, **126**: 97 (1983)
25 W. Melnitchouk and A. W. Thomas, Phys. Rev. D, **47**: 3794 (1993)
26 S. J. Brodsky and B. Q. Ma, Phys. Lett. B, **381**: 317 (1996)
27 H. Holtmann, A. Szczurek, and J. Speth, Nucl. Phys. A, **596**: 631 (1996) [arXiv:9601388 [hep-ph]]
28 S. Kumano, Phys. Rept., **303**: 183 (1998)
29 G. T. Garvey and J. C. Peng, Prog. Part. Nucl. Phys., **47**: 203 (2001)
30 F. G. Cao and A. I. Signal, Phys. Lett. B, **559**: 229 (2003)
31 M. Traini, Phys. Rev. D, **89**: 034021 (2014) [arXiv:1309.5814 [hep-ph]]
32 A. Vega, I. Schmidt, T. Gutsche, and V. E. Lyubovitskij, Phys. Rev. D, **93**: 056001 (2016)
33 E. Hoffmann and R. Moore, Z. Phys. C, **20**: 71 (1983)
34 B. W. Harris, J. Smith, and R. Vogt, Nucl. Phys. B, **461**: 181 (1996) [arXiv:9508403 [hep-ph]]
35 J. Pumplin, H. L. Lai, and W. K. Tung, Phys. Rev. D, **75**: 054029 (2007) [arXiv:0701220 [hep-ph]]
36 P. M. Nadolsky, H. L. Lai, Q. H. Cao, J. Huston, J. Pumplin, D. Stump, W. K. Tung, and C.-P. Yuan, Phys. Rev. D, **78**: 013004 (2008) [arXiv:0802.0007 [hep-ph]]
37 S. Dulat, T. J. Hou, J. Gao, J. Huston, J. Pumplin, C. Schmidt, D. Stump, and C.-P. Yuan, Phys. Rev. D, **89**: 073004 (2014) [arXiv:1309.0025 [hep-ph]]
38 P. Jimenez-Delgado, T. J. Hobbs, J. T. Londergan, and W. Melnitchouk, Phys. Rev. Lett., **114**: 082002 (2015) [arXiv:1408.1708 [hep-ph]]
39 S. J. Brodsky and S. Gardner, Phys. Rev. Lett., **116**: 019101 (2016) [arXiv:1504.00969 [hep-ph]]
40 R. D. Ball et al (NNPDF Collaboration), arXiv:1605.06515 [hep-ph]
41 W. C. Chang and J. C. Peng, Phys. Rev. Lett., **106**: 252002 (2011).
42 W. C. Chang and J. C. Peng, Phys. Lett. B, **704**: 197 (2011) [arXiv:1105.2381 [hep-ph]]
43 W. C. Chang and J. C. Peng, Phys. Rev. D, **92**: 054020 (2015) [arXiv:1410.7027 [hep-ph]]
44 V. A. Bednyakov, M. A. Demichev, G. I. Lykasov, T. Stavreva, and M. Stockton, Phys. Lett. B, **728**: 602 (2014) [arXiv:1305.3548 [hep-ph]]
45 S. Rostami, A. Khorramian, A. Aleedaneshvar, and M. Goharipour, J. Phys. G, **43**: 055001 (2016) [arXiv:1510.08421 [hep-ph]]
46 F. Lyonnet, A. Kusina, T. Jeo, K. Kovark, F. Olness, I. Schienbein, and J. Y. Yu, JHEP, **1507**: 141 (2015) [arXiv:1504.05156 [hep-ph]]
47 P. H. Beauchemin, V. A. Bednyakov, G. I. Lykasov, and Y. Y. Stepanenko, Phys. Rev. D, **92**: 034014 (2015) [arXiv:1410.2616 [hep-ph]]
48 T. Boettcher, P. Ilten, and M. Williams, Phys. Rev. D, **93**: 074008 (2016) [arXiv:1512.06666 [hep-ph]]
49 A. V. Lipatov, G. I. Lykasov, Y. Y. Stepanenko, and V. A. Bednyakov, arXiv:1606.04882 [hep-ph]
50 S. Duan, C. S. An, and B. Saghai, Phys. Rev. D, **93**: 114006 (2016) [arXiv:1606.02000 [hep-ph]]
51 J. Pumplin, Phys. Rev. D, **73**: 114015 (2006) [arXiv:0508184 [hep-ph]]
52 T. J. Hobbs, J. T. Londergan, and W. Melnitchouk, Phys. Rev. D, **89**: 074008 (2014) [arXiv:1311.1578 [hep-ph]]

53 M. Salajegheh, Phys. Rev. D, **92**: 074033 (2015)
54 R. D. Ball, V. Bertone, M. Bonvini, S. Forte, P. Groth Merrild, J. Rojo, and L. Rottoli, Phys. Lett. B, **754**: 49 (2016) [arXiv:1510.00009 [hep-ph]]
55 R. Laha and S. J. Brodsky, arXiv:1607.08240 [hep-ph]
56 W. C. Chang and J. C. Peng, Prog. Part. Nucl. Phys., **79**: 95 (2014)
57 S. J. Brodsky, A. Kusina, F. Lyonnet, I. Schienbein, H. Spiesberger, and R. Vogt, Adv. High Energy Phys., **2015**: 231547 (2015) [arXiv:1504.06287 [hep-ph]]
58 S. J. Brodsky, hep-ph/0412101
59 J. F. Donoghue and E. Golowich, Phys. Rev. D, **15**: 3421 (1977)
60 J. Badier et al (NA3 Collaboration), Z. Phys. C, **20**: 101 (1983)
61 P. Chauvat et al (R608 Collaboration), Phys. Lett. B, **199**: 304 (1987)
62 M. J. Leitch et al (NuSea Collaboration), Phys. Rev. Lett., **84**: 3256 (2000) [nucl-ex/9909007]
63 E. M. Aitala et al (E791 Collaboration), Phys. Lett. B, **495**: 42 (2000) [hep-ex/0008029]
64 E. M. Aitala et al (E791 Collaboration), Phys. Lett. B, **539**: 218 (2002) [hep-ex/0205099]
65 V. M. Abazov et al (D0 Collaboration), Phys. Rev. Lett., **112**: 042001 (2014) [arXiv:1308.4384 [hep-ex]]
66 G. P. Lepage and S. J. Brodsky, Phys. Lett. B, **87**: 359 (1979)
67 G. P. Lepage and S. J. Brodsky, Phys. Rev. D, **22**: 2157 (1980)
68 T. Aaltonen et al (CDF Collaboration), Phys. Rev. D, **81**: 052006 (2010) [arXiv:0912.3453 [hep-ex]]
69 V. M. Abazov et al (D0 Collaboration), Phys. Lett. B, **714**: 32 (2012) [arXiv:1203.5865 [hep-ex]]
70 J. Alwall, M. Herquet, F. Maltoni, O. Mattelaer, and T. Stelzer, JHEP, **1106**: 128 (2011) [arXiv:1106.0522 [hep-ph]]
71 Program summary: http://particles.ipm.ir/links/QCD.htm
72 D. Bourilkov, R. C. Group, and M. R. Whalley, hep-ph/0605240
73 M. Botje, Comput. Phys. Commun., **182**: 490 (2011) [arXiv:1005.1481 [hep-ph]]
74 A. Kusina, K. Kovaik, T. Jeo, D. B. Clark, F. I. Olness, I. Schienbein, and J. Y. Yu, PoS DIS, **2014**: 047 (2014) [arXiv:1408.1114 [hep-ph]]